

Urchin-Shaped Manganese Oxide Nanoparticles as pH-Responsive Activatable T_1 Contrast Agents for Magnetic Resonance Imaging**

Taekhoon Kim, Eun-Jin Cho, Youngjoo Chae, Minsik Kim, Aram Oh, Juhong Jin, Eun-Sook Lee, Hionsuck Baik, Seungjoo Haam, Jin-Suck Suh, Yong-Min Huh,* and Kwangyeol Lee*

The ultrasensitive detection of cancer in its earliest stage would greatly help the ensuing treatment process, and therefore various imaging modalities and image-enhancing methods are being developed.^[1] In particular, metal oxide nanoparticles prove to be promising contrast agents in magnetic resonance imaging (MRI) for the ultrasensitive detection of cancer, and the principles for enhancing MRI contrast have been deciphered recently.^[2] For example, it is advantageous to employ superparamagnetic metal oxide nanoparticles with high magnetization values (emu g^{-1}) for improved T_2 image contrast.^[3] In addition, clusters of superparamagnetic nanoparticles exhibit greater T_2 contrast abilities than individual nanoparticles.^[4] Therefore, the clustering of magnetic nanoparticles with high magnetization values is advantageous because of both improved T_2 contrast and the frugal usage of targeting moieties. For enhanced T_1 contrast, nanoparticles should have numerous high-spin metal ions exposed on the surface for facilitated interactions with the

surrounding water molecules.^[5,6] This calls for the use of smaller nanoparticles with a high surface-to-volume ratio, but simply using a high number of small nanoparticles is not compatible with the frugal usage of targeting moieties. In the case of large nanoparticles, the non-exposed metal ions in the core cannot contribute to the MRI T_1 contrast; the T_1 -weighted image obtained with metal ions is much poorer than that from conventional ion-based contrast agents.

We reasoned that the highest surface area for a nanoparticle of a given diameter would be provided by an urchin-like morphology as shown in Figure 1. As a model system to prove our concept, manganese oxides were investigated that had been previously used as an MRI T_1 contrast agent. This system is particularly interesting because of the easy conversion of MnO to Mn_3O_4 and the different stabilities of these two manganese oxide phases under physiological conditions. It is envisaged that the MnO nanoparticle trapped in the thin shell of an urchin-shaped stable Mn_3O_4 phase can be unloaded in the form of Mn^{II} ions to the low-pH sites ($< \text{pH } 7$) in the tumor. While the low pH of tumor cells has been exploited for the fabrication of numerous activatable drug-delivery systems,^[7] a nanoparticle-based pH-activatable MRI agent is unprecedented to our knowledge. The combination of the T_1 contrast effect from the empty Mn_3O_4 urchin shell with a high surface area and the released Mn^{II} ions should make the $\text{MnO}@\text{Mn}_3\text{O}_4$ nanourchin a powerful MRI T_1 contrast agent. Herein we report the synthesis of the $\text{MnO}@\text{Mn}_3\text{O}_4$ nanourchin through facet-selective etching as well as its successful application as a pH-responsive activatable T_1 contrast agent,

[*] T. Kim,^[†] Y. Chae, M. Kim, A. Oh, J. Jin, Prof. K. Lee

Department of Chemistry, Korea University

Seoul 136-701 (Korea)

E-mail: kylee1@korea.ac.kr

E.-S. Lee, Prof. J.-S. Suh, Prof. Y.-M. Huh

YUHS-KRIBB Medical Convergence Research Institute

Yonsei University, Seoul 120-752 (Korea)

E-mail: ymhuh@yuhs.ac

Prof. Y.-M. Huh

Severance Biomedical Science Institute

Yonsei University (Korea)

E.-J. Cho,^[†]

Program for Nanomedical Science and Technology

Yonsei University (Korea)

E.-J. Cho,^[†] E.-S. Lee, Prof. J.-S. Suh, Prof. Y.-M. Huh

Department of Radiology & Department of Biochemistry and

Molecular Biology, Yonsei University (Korea)

Dr. H. Baik

Korea Basic Science Institute (KBSI)

Seoul 136-713 (Korea)

Prof. S. Haam

Department of Chemical and Biomolecular Engineering

Yonsei University, Seoul 120-749 (Korea)

[†] These authors contributed equally.

[**] This work was supported by MIHWAF (the Korea Health21 R&D Project: A090728) and KRIBB Research Initiative Program. We thank KBSI for use of their HRTEM, XPS, ICP-AES instruments, and Prof. Sang-Won Lee (Korea University) for MS measurements.

Supporting information for this article is available on the WWW under <http://dx.doi.org/10.1002/anie.201103108>.

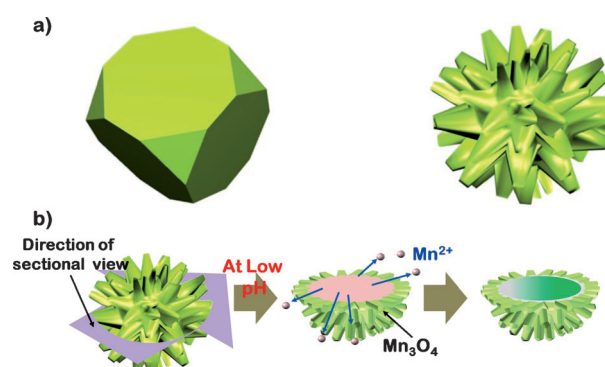


Figure 1. a) Schematic diagram of a low-surface-area truncated cube and a high-surface-area urchin. b) Representation of the unloading of core MnO content from the urchin-shaped $\text{MnO}@\text{Mn}_3\text{O}_4$ nanoparticle at low pH.

which is compatible with the frugal usage of cancer-targeting moieties.

Our strategy to form manganese oxide nanourchins entails the formation of large polycrystalline MnO nanoparticles (150–200 nm) and subsequent anisotropic etching of the nanocrystal facets. In a typical synthesis, a solution of $\text{Mn}(\text{CH}_3\text{COO})_2$ (1.4 mmol, Aldrich, 98%), oleylamine (3.0 mmol, 2.14 equiv), and oleic acid (1.5 mmol, 1.07 equiv) in trioctylamine (TOA, 6.2 mL) was prepared in 100 mL Schlenk tube equipped with a bubbler and an N_2 line (flow rate $40 \text{ cm}^3 \text{ min}^{-1}$). The Schlenk tube was heated to 270°C at a rate of $18^\circ\text{C min}^{-1}$ in an oil bath. After 1 h at 270°C , the formation of large MnO nanoparticles was complete. Large nanoparticles were composed of a number of attached smaller {111}-faceted, octahedral MnO nanoparticles (Figure 2a). These polycrystalline MnO nanoparticles were subjected to facet-selective etching by oleic acid. Specifically, in order to effect the anisotropic etching, oleic acid (1.6 mmol, 1.14 equiv) and TOA (1.24 mL) were added to the reaction mixture, and the resulting solution was heated further at 270°C for 1 h.

The product morphology and structure were analyzed by transmission electron microscopy (TEM) and high-resolution TEM (HRTEM; Figure 2). The urchin-like shape of the product is clearly visible, with blocks of spikes aligned in the same directions. While anisotropic etching has been successfully employed in the fabrication of Si devices,^[8] anisotropic etching of nanoparticles is uncommon.^[9] Detailed analysis (Figure S2 in the Supporting Information) shows that the {111} facets of the MnO nanocrystal are most resistant to the etching, as judged from the fact that the spikes with {111} directions remain.

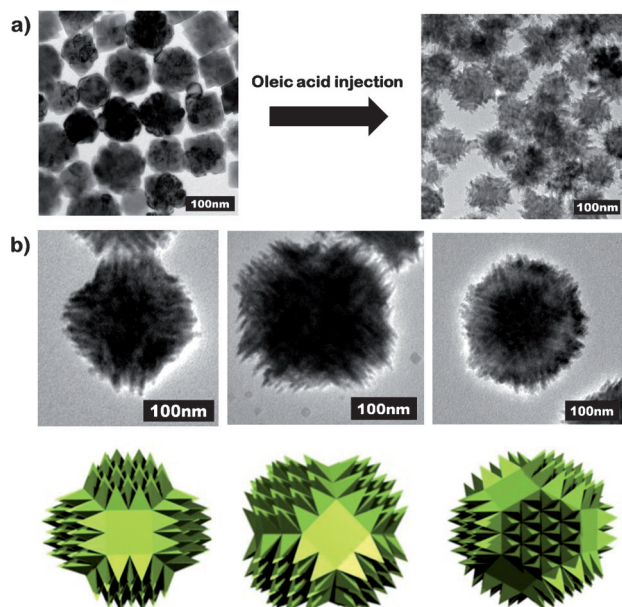


Figure 2. TEM images of a) the conversion of polycrystalline octahedral MnO nanoparticles into urchin-shaped MnO nanocrystals by an anisotropic etching process, b) urchin-shaped nanocrystals from different viewpoints and corresponding schematic images in green.

The surface of the MnO nanourchin undergoes a fast oxidation to form a $t\text{-Mn}_3\text{O}_4$ phase under ambient conditions, as indicated by the XPS analysis (see Figure S7 in the Supporting Information). Once the surface is passivated by the formed $t\text{-Mn}_3\text{O}_4$ phase, the MnO trapped inside is preserved for a prolonged period in the air. However, the oxidation is much facilitated in aqueous solutions (vide infra). In order to examine the pH-dependent stability of the formed $\text{MnO@Mn}_3\text{O}_4$ nanourchin, we placed MnO nanourchins surface-modified with carboxylated amphiphilic polysorbate 80 molecules^[10] in phosphate-buffered saline (PBS) solutions of various pH values. While the nanourchin is very stable at pH values above 7, the MnO core is easily dissolved at lower pH conditions (pH 4–6) to give a hollow Mn_3O_4 nanourchin (Figure S13 in the Supporting Information). Interestingly, even the Mn_3O_4 spiked shell part can be dissolved at $\text{pH} < 3$, indicating that the entire nanostructure could disintegrate within a cell, which can possess domains with very low pH values.

The relevance of Mn^{II} ion leaching to the MRI T_1 imaging was investigated by obtaining temporal MRI T_1 contrast images of $\text{MnO@Mn}_3\text{O}_4$ nanourchins in a buffer solution at pH 5 (Figure 3). At pH 5, the structure of the hollow nanourchin is stable, consistent with the TEM analysis of morphological change. As judged by the inductively coupled plasma (ICP) analysis, the Mn^{II} ions that leached out within 48 h constitute about 16% of the total Mn content of the nanourchin structure (Figure 3a). As described in the Supporting Information, prolonged treatment under aqueous conditions converts most of the MnO phase into Mn_3O_4 .

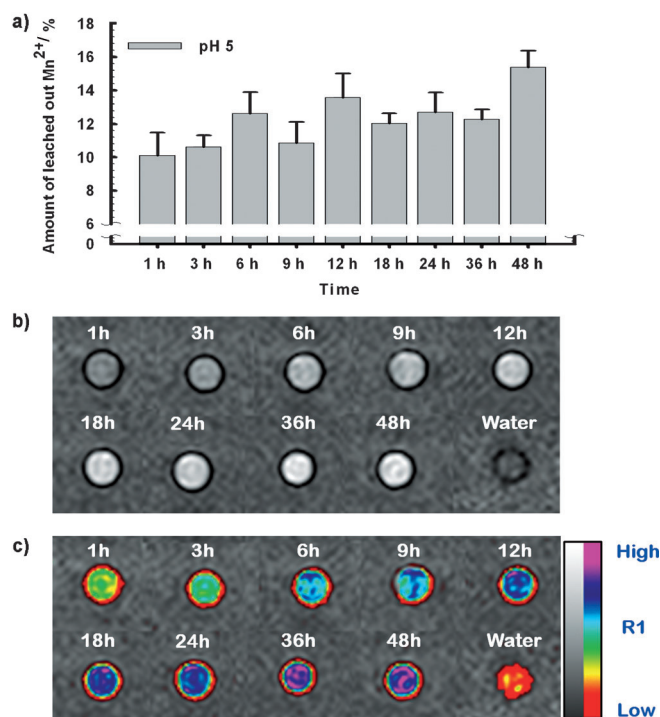


Figure 3. a) Percentage of Mn^{II} ion leached out from $\text{MnO@Mn}_3\text{O}_4$ nanourchins at pH 5. b) Solution magnetic resonance (MR) images of leached out solution from pH 5 PBS buffer and c) the respective color-coded images in (b).

However, even with this small remaining MnO content, the T_1 contrast is greatly enhanced owing to the accumulation of released Mn^{II} ions from gradually disintegrating MnO (Figure 3b,c).

Having observed the stability of the nanourchins at various pH levels and the relevance of released Mn^{II} ions to the MRI T_1 contrast, we investigated the stability of the nanourchins in macrophages and cancer cells. Invariably, completely emptied nanourchins started to appear starting 3 h after uptake, and the formed hollow Mn_3O_4 nanourchins slowly disintegrated over time (see Figure S16 in the Supporting Information); the spike parts appear to be the most stable in the nanourchin structure. This result suggests that macrophages and cancer cells are capable of dissolving the MnO phase, and even the Mn_3O_4 phase at a lower rate, in intracellular low-pH domains. It appears that cells are capable of removing Mn^{II} ions that are not required in large quantity for normal cell functions. The brightest T_1 images were observed for NIH3T6.7 cells treated with humanized anti-HER2 antibody (Herceptin)-modified $MnO@Mn_3O_4$ nanourchins for 30 min. Extended treatment with the $MnO@Mn_3O_4$ nanourchins led only to reduced T_1 imaging ability, indicating a continuous purging of Mn^{II} ions out of the cancer cells. Because of this Mn^{II} removal process, $MnO@Mn_3O_4$ nanourchins and hollow Mn_3O_4 nanourchins, at the same nanoparticle counts, show little difference in MRI T_1 contrasts for treated cancer cells. While the purged Mn^{II} ions do not contribute to the *in vitro* T_1 imaging of cancer cells, they could meet the following fates in tumor tissue: the purged Mn^{II} ions might be retained in the tumor tissue by diffusion into the extracellular domain, or they may move into the blood stream to be completely cleared out from the tumor tissue. If the former route is not negligible, then the entire tumor tissue, even the interior of the tumor mass, would be imagable by the MRI T_1 mode.^[11]

In order to investigate the ability of manganese ions released from the $MnO@Mn_3O_4$ nanourchins to image tumors, we performed *in vivo* MRI experiments with a mouse tumor model established by implanting NIH3T6.7 cells in the proximal thigh region of a mouse (Figure 4). $MnO@Mn_3O_4$ nanourchins or Mn_3O_4 hollow nanourchins, both modified with anti-HER2 antibodies, were intravenously injected into the mouse tail vein. The nanoparticle counts for both nanostructures were kept equal for the *in vivo* study. If the core MnO part in a $MnO@Mn_3O_4$ nanourchin is eventually removed, the resulting morphology would be the same as the Mn_3O_4 hollow nanourchin, and therefore any difference in MR imaging ability would be due to both the leached out Mn^{II} ions from the $MnO@Mn_3O_4$ nanourchin and the ability of the tumor tissue to retain the Mn^{II} ions (or release them into blood stream). Also, the number concentration of manganese nanourchins was deliberately controlled so that the hollow Mn_3O_4 nanourchin does not show a significant T_1 contrast. If there is any T_1 contrast effect from the $MnO@Mn_3O_4$ nanourchin, the effect should be solely attributed to the leached out manganese ions.

Consistent with the instability of MnO under low-pH conditions and the accompanied release of manganese ions, the MR T_1 imaging ability of $MnO@Mn_3O_4$ nanourchins was

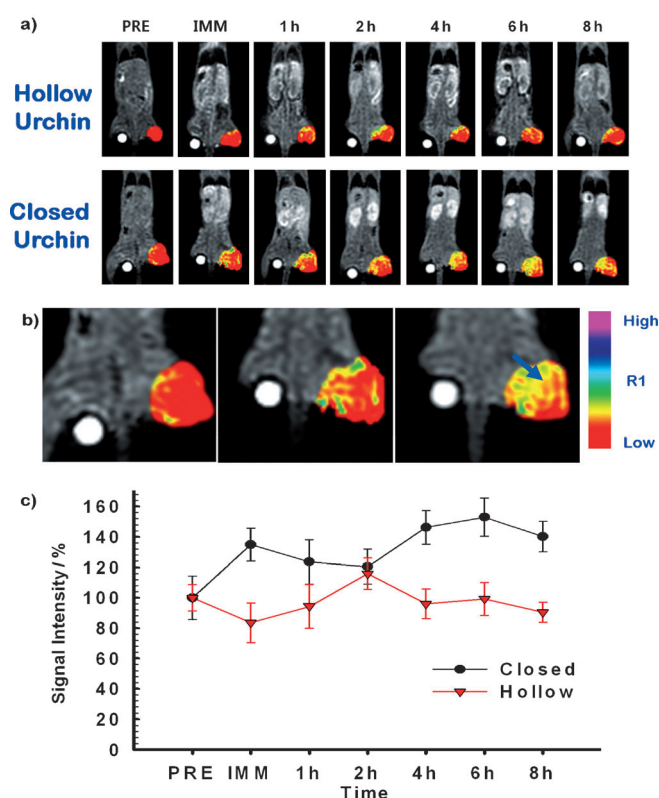


Figure 4. a) Temporal color-coded T_1 -ultrashort echo time MR images of tumor after intravenous injection of hollow Mn_3O_4 nanourchin-HER (hollow urchin) and $MnO@Mn_3O_4$ nanourchin-HER (closed urchin). b) Magnified view of tumor MR images of preinjection (left), immediately after injection (middle), and 6 h after injection (right); the arrow indicates the diffusion direction of Mn^{II} ion. c) Plot of signal intensity ($R_{1,sh}/R_{1,pre} \times 100\%$) versus time after the injection of hollow Mn_3O_4 nanourchin-HER (red triangles) and $MnO@Mn_3O_4$ nanourchin-HER (black circles).

far superior to that of hollow Mn_3O_4 nanourchins. While the T_1 contrast of the tumor treated with hollow Mn_3O_4 nanourchins did not change over time, the tumor treated with $MnO@Mn_3O_4$ showed much enhanced T_1 contrast after 4 h. Close examination of the tumor MR images after 4 h revealed that the MR contrast enhancement is visible not only in the periphery but also in the tumor interior; only the vacuatures in the periphery are visible in the initial stage. This clearly demonstrates that the MnO content in $MnO@Mn_3O_4$ is destabilized by the low-pH conditions in the tumor, Mn^{II} ions are released, and ions migrate into the tumor interior plausibly through a diffusion process. We also established that the enhanced contrast effect can be achieved with only about (70 ± 35) ng of released Mn ions per tumor in the mouse (see Figure S23 in the Supporting Information). Further study is under way to thoroughly assess the MRI T_1 contrast ability of Mn^{II} ions liberated from the MnO phase. It is tempting to employ very small MnO nanoparticles with high surface area as ion-delivery vehicles, considering the small amount of manganese ions required for enhanced MRI contrast. However, very small MnO nanoparticles are easily further oxidized to the Mn_3O_4 phase during the water-

solubilization step (see Figure S24 in the Supporting Information), and are therefore not suitable as ion-delivery vehicles. Also, the small nanoparticles require nonfrugal usage of targeting moieties, making them further unattractive as ion-delivery vehicles.

The current study has the following important implications. While cancer cells might effectively pump out potentially toxic Mn^{II} ions, the Mn^{II} ion purging does not appear to be unidirectional to the vasculatures. Recently, Fe ions leached out from FePt have been utilized for tumoricidal effect.^[12] Our finding of the metal-ion-induced MRI contrast enhancing effect within the tumor mass seems to further substantiate the observed tumoricidal effect of FePt nanoparticles by means of leached out iron ions. Metal oxide nanoparticles have been recently utilized for T_1 MR imaging.^[13] The instability of MnO in cancer cells as revealed by this study, however, implies that the T_1 MRI contrast might be caused by the released metal ions, not just the high surface/volume ratio of small metal oxide nanoparticles. Therefore, the MRI imaging ability of metal-oxide-based imaging agents has to be assessed in conjunction with the accompanied potential toxicity of the leached out metal ions.

In summary, we have demonstrated a new concept for MRI contrast agents by utilizing the different stabilities of metal oxides under low-pH conditions. Specifically, the unstable MnO phase trapped by a stable urchin-shaped Mn_3O_4 hollow container, synthesized by anisotropic etching, is delivered to tumor in an efficient manner. Upon arrival in the tumor, MnO, which is unstable at low pH, is dismantled to release Mn^{II} ions in the low-pH sites of the tumor cells. The Mn^{II} ions randomly diffuse within the tumor mass and this leads to a complete mapping of the tumor morphology. The hollow nanourchin Mn_3O_4 developed in this study might be further utilized, but with a further optimization in size and surface functionalization for an enhanced duration in blood circulation, as a stable T_1 contrast agent. Furthermore, other anticancer drugs or well-established metal-ion-based imaging moieties might be loaded into the nanourchin hollow containers and delivered to tumors with a frugal usage of targeting moieties. We are currently investigating these possibilities.

Received: May 5, 2011

Published online: September 16, 2011

Keywords: anisotropic etching · crystal growth · magnetic resonance imaging · manganese · nanoparticles

- [1] a) J. B. Haun, C. M. Castro, R. Wang, V. M. Peterson, B. S. Marinelli, H. Lee, R. Weissleder, *Sci. Transl. Med.* **2011**, *3*, 71ra16; b) H. Shao, T.-J. Yoon, M. Liong, R. Weissleder, H. Lee, *Beilstein J. Nanotechnol.* **2010**, *1*, 142–154; c) E. Tasciotti, X. Liu, R. Bhavane, K. Plant, A. D. Leonard, B. K. Price, M. M.-C. Cheng, P. Decuzzi, J. M. Tour, F. Robertson, M. Ferrari, *Nat. Nanotechnol.* **2008**, *3*, 151–157; d) W. A. Kalender, *Phys. Med. Biol.* **2006**, *51*, R29–R43; e) G. Michael, *Phys. Educ.* **2001**, *36*, 442–451.
- [2] a) H. B. Na, I. C. Song, T. Hyeon, *Adv. Mater.* **2009**, *21*, 2133–2148; b) J.-H. Lee, Y.-M. Huh, Y.-w. Jun, J.-w. Seo, J.-t. Jang, H.-T. Song, S. Kim, E.-J. Cho, H.-G. Yoon, J.-S. Suh, J. Cheon, *Nat. Med.* **2007**, *13*, 95–99; c) H. Lee, M. K. Yu, S. Park, S. Moon, J. J. Min, Y. Y. Jeong, H.-W. Kang, S. Jon, *J. Am. Chem. Soc.* **2007**, *129*, 12739–12745; d) H. Lee, E. Lee, D. K. Kim, N. K. Jang, Y. Y. Jeong, S. Jon, *J. Am. Chem. Soc.* **2006**, *128*, 7383–7389.
- [3] Y.-w. Jun, J.-H. Lee, J. Cheon, *Angew. Chem.* **2008**, *120*, 5200–5213; *Angew. Chem. Int. Ed.* **2008**, *47*, 5122–5135.
- [4] a) S. A. Corr, S. J. Byrne, R. Tekoriute, C. J. Meledandri, D. F. Brougham, M. Lynch, C. Kerskens L. O'Dwyer and Y. K. Gun'ko, *J. Am. Chem. Soc.* **2008**, *130*, 4214–4215; b) J.-H. Park, G. von Maltzahn, L. Zhang, M. P. Schwartz, E. Ruoslahti, S. N. Bhatia, M. J. Sailor, *Adv. Mater.* **2008**, *20*, 1630–1635; c) J. Yang, C.-H. Lee, H.-J. Ko, J.-S. Suh, H.-G. Yoon, K. Lee, Y.-M. Huh, S. Haam, *Angew. Chem.* **2007**, *119*, 8992–8995; *Angew. Chem. Int. Ed.* **2007**, *46*, 8836–8839; d) T. J. Harris, G. v. Maltzahn, A. M. Derfus, E. Ruoslahti, S. N. Bhatia, *Angew. Chem.* **2006**, *118*, 3233–3237; *Angew. Chem. Int. Ed.* **2006**, *45*, 3161–3165.
- [5] a) H. B. Na, T. Hyeon, *J. Mater. Chem.* **2009**, *19*, 6267–6273; b) J. Shin, R. M. Anisur, M. K. Ko, G. H. Im, J. H. Lee, I. S. Lee, *Angew. Chem.* **2009**, *121*, 327–330; *Angew. Chem. Int. Ed.* **2009**, *48*, 321–324; c) H. B. Na, J. H. Lee, K. An, Y. I. Park, M. Park, I. S. Lee, D.-H. Nam, S. T. Kim, S.-H. Kim, S.-W. Kim, K.-H. Lim, K.-S. Kim, S.-O. Kim, T. Hyeon, *Angew. Chem.* **2007**, *119*, 5493–5497; *Angew. Chem. Int. Ed.* **2007**, *46*, 5397–5401.
- [6] a) Y.-s. Yoon, B.-i. Lee, K. S. Lee, G. H. Im, S.-H. Byeon, J. H. Lee, I. S. Lee, *Adv. Funct. Mater.* **2009**, *19*, 3375–3380; b) J. Y. Park, M. J. Baek, E. S. Choi, S. Woo, J. H. Kim, T. J. Kim, J. C. Jung, K. S. Chae, Y. Chang, G. H. Lee, *ACS Nano* **2009**, *3*, 3663–3669; c) J.-L. Bridot, A.-C. Faure, S. Laurent, C. Rivière, C. Billotey, B. Hiba, M. Janier, V. Jossierand, J.-L. Coll, L. V. Elst, R. Muller, S. Roux, P. Perriat, O. Tillement, *J. Am. Chem. Soc.* **2007**, *129*, 5076–5084.
- [7] a) T. Kim, Y.-M. Huh, S. Haam, K. Lee, *J. Mater. Chem.* **2010**, *20*, 8194–8206; b) E. Gullotti, Y. Yeo, *Mol. Pharm.* **2009**, *6*, 1041–1051; c) J. A. MacKay, M. Chen, J. R. McDaniel, W. Liu, A. J. Simnick, A. Chilkoti, *Nat. Mater.* **2009**, *8*, 993–999; d) W. Wei, G.-H. Ma, G. Hu, D. Yu, T. Mcleish, Z.-G. Su, Z.-Y. Shen, *J. Am. Chem. Soc.* **2008**, *130*, 15808–15810; e) T. T. Morgan, H. S. Muddana, E. İ. Altinoğlu, S. M. Rouse, A. Tabaković, T. Tabouillot, T. J. Russin, S. S. Shanmugavelandy, P. J. Butler, P. C. Eklund, J. K. Yun, M. Kester, J. H. Adair, *Nano Lett.* **2008**, *8*, 4108–4115.
- [8] a) K. Peng, A. Lu, R. Zhang, S.-T. Lee, *Adv. Funct. Mater.* **2008**, *18*, 3026–3035; b) C. C. Striemer, R. Krishnan, P. M. Fauchet, L. Tsybeskov, *Nano Lett.* **2001**, *1*, 643–646; c) C. Marzolin, S. P. Smith, M. Prentiss, G. M. Whitesides, *Adv. Mater.* **1998**, *10*, 571–574; d) O. Tabata, R. Asahi, H. Funabashi, K. Shimaoka, S. Sugiyama, *Sens. Actuators A* **1992**, *34*, 51–57.
- [9] a) M. J. Mulvihill, X. Y. Ling, J. Henzie, P. Yang, *J. Am. Chem. Soc.* **2010**, *132*, 268–274; b) H. Kim, Y. Chae, D. H. Lee, M. Kim, J. Huh, Y. Kim, H. Kim, H. J. Kim, S. O. Kim, H. Baik, K. Choi, J. S. Kim, G.-R. Yi, K. Lee, *Angew. Chem.* **2010**, *122*, 5848–5852; *Angew. Chem. Int. Ed.* **2010**, *49*, 5712–5716; c) M. S. Yavuz, Y. Cheng, J. Chen, C. M. Cobley, Q. Zhang, M. Rycenga, J. Xie, C. Kim, K. H. Song, A. G. Schwartz, L. V. Wang, Y. Xia, *Nat. Mater.* **2009**, *8*, 935–939; d) K. An, S. G. Kwon, M. Park, H. B. Na, S.-I. Baik, J. H. Yu, D. Kim, J. S. Son, Y. W. Kim, I. C. Song, W. K. Moon, H. M. Park, T. Hyeon, *Nano Lett.* **2008**, *8*, 4252–4258.
- [10] E.-J. Cho, J. Yang, K. A. Mohamedali, E.-K. Lim, E.-J. Kim, C. J. Farhangfar, J.-S. Suh, S. Haam, M. G. Rosenblum, Y.-M. Huh, *Invest. Radiol.* **2011**, *46*, 441–449.
- [11] a) L. Zhang, X. Zhong, L. Wang, H. Chen, Y. A. Wang, J. Yeh, L. Yang, H. Mao, *J. Magn. Reson. Imaging* **2011**, *33*, 194–202; b) C. T. Farrar, G. Dai, M. Novikov, A. Rosenzweig, R. Weissleder, B. R. Rosen, D. E. Sosnovik, *NMR Biomed.* **2008**, *21*, 453–463; c) M. Stuber, W. D. Gilson, M. Schär, D. A. Kedziorek, L. V. Hofmann, S. Shah, E.-J. Vonken, J. W. M. Bulte, D. L. Kraitchman, *Magn. Reson. Med.* **2007**, *58*, 1072–1077.

- [12] C. Xu, Z. Yuan, N. Kohler, J. Kim, M. A. Chung, S. Sun, *J. Am. Chem. Soc.* **2009**, *131*, 15346–15351.
- [13] a) H. Yang, Y. Zhuang, H. Hu, X. Du, C. Zhang, X. Shi, H. Wu, S. Yang, *Adv. Funct. Mater.* **2010**, *20*, 1733–1741; b) U. I. Tromsdorf, O. T. Bruns, S. C. Salmen, U. Beisiegel, H. Weller, *Nano Lett.* **2009**, *9*, 4434–4440; c) T. Yu, J. Moon, J. Park, Y. I. Park, H. B. Na, B. H. Kim, I. C. Song, W. K. Moon, T. Hyeon, *Chem. Mater.* **2009**, *21*, 2272–2279; d) I.-F. Li, C.-H. Su, H.-S. Sheu, H.-C. Chiu, Y.-W. Lo, W.-T. Lin, J.-H. Chen, C.-S. Yeh, *Adv. Funct. Mater.* **2008**, *18*, 766–776.
-